Effects of magnetic field orientation on optical decoherence in $Er^{3+}:Y_2SiO_5$

Thomas Böttger*
Department of Physics and Astronomy, University of San Francisco, 2130 Fulton Street, San Francisco, California 94117, USA and Department of Physics, Montana State University, Bozeman, Montana 59717, USA

C. W. Thiel† and R. L. Cone‡
Department of Physics, Montana State University, Bozeman, Montana 59717, USA

Y. Sun§
Department of Physics, Montana State University, Bozeman, Montana 59717, USA and Department of Physics, University of South Dakota, Vermillion, South Dakota 57069, USA

(Received 31 October 2008; published 10 March 2009)

The influence of the anisotropic Zeeman effect on optical decoherence was studied for the 1.54 μm telecom transition in $Er^{3+}:Y_2SiO_5$ using photon echo spectroscopy as a function of applied magnetic field orientation and strength. The decoherence strongly correlates with the Zeeman energy splittings described by the ground- and excited-state g factor variations for all inequivalent Er^{3+} sites, with the observed decoherence times arising from the combined effects of the magnetic dipole-dipole coupling strength and the ground- and excited-state spin-flip rates, along with the natural lifetime of the upper level. The decoherence time was maximized along a preferred magnetic field orientation that minimized the effects of spectral diffusion and that enabled the measurement of an exceptionally narrow optical resonance in a solid—demonstrating a homogeneous linewidth as narrow as 73 Hz.

DOI: 10.1103/PhysRevB.79.115104 PACS number(s): 42.50.Md, 76.30.Kg, 78.47.jf, 42.50.Ex

I. INTRODUCTION

Understanding and minimizing decoherence in resonant optical materials is one of the outstanding questions in optical materials research as well as quantum information science. This paper addresses that issue by exploring the anisotropic effects of applied magnetic fields on optical decoherence in rare-earth-ion-doped solids where light can be used to prepare qubits and manipulate quantum states.

Unusual optical properties enable the material $Er^{3+}:Y_2SiO_5$ to play an important role in rare-earth based spatial spectral holography (SSH) and spectral hole burning (SHB) as well as in quantum cryptography and quantum computing applications, employing the 1.54 μm telecommunication transition where abundant commercial off-the-shelf optical hardware is available and inexpensive. These applications require low decoherence rates to maximize the length of time over which phase-coherent interactions with the material may be maintained. These decoherence times, or phase memory lifetimes, determine the ultimate length of a data train that can be stored or processed by the SSH and SHB material and the number of quantum gate operations that may be performed in a quantum information system. In the frequency domain picture, the very sharp optical resonances corresponding to these low levels of decoherence can serve as narrow data channels or frequency references. The material system $Er^{3+}:Y_2SiO_5$ has been shown to meet the requirements for a wide variety of optical devices and was successfully utilized in demonstrations of laser frequency stabilization,[1–5] wideband signal processing,[6] all-optical correlators,[7,8] and radio-frequency spectral analysis.[9] By combining narrow homogeneous linewidths with wide inhomogeneous absorption lines, which can be tailored to tens of gigahertz in $Er^{3+}:Y_2SiO_5$ by codoping Eu^{3+} ions,[10] the material attains exceptional processing power as many parallel data channels can be addressed across the inhomogeneous absorption line. The time-bandwidth product is the relevant figure of merit for these applications, with an upper limit approaching 10^8 that is set by the ratio of the inhomogeneous absorption linewidth to the homogeneous linewidth Γ_{inh}/Γ_h. Recently $Er^{3+}:Y_2SiO_5$ has been considered as a promising candidate for demonstrating qubits and quantum memories[11–13] with the added advantage that the communication wavelength would allow the transfer of qubits over long distances.

To both optimize $Er^{3+}:Y_2SiO_5$ for these applications and improve our fundamental understanding of decoherence in general, extensive material research has been carried out. Previously, we have reported site-selective spectroscopic studies of the $^4I_{15/2} \leftrightarrow {}^4I_{13/2}$ transition, providing detailed knowledge of the crystal-field level structure and excited-state lifetimes.[14] Optical decoherence was also studied with stimulated-photon echo spectroscopy as a function of crystal temperature, Er^{3+}-dopant concentration, and magnetic field strength, gaining insight into the mechanisms of spectral diffusion and the underlying nanospin dynamics responsible for the decoherence of the transition.[15] We have also presented the complete magnetic g tensors for the lowest-energy $^4I_{15/2}$ and $^4I_{13/2}$ states in $Er^{3+}:Y_2SiO_5$ for both crystallographic sites deduced from orientation-dependent optical Zeeman spectroscopy over three orthogonal crystal planes,[16] complementing the EPR work by Noël *et al.*[11]

Recently, $Er^{3+}:Y_2SiO_5$ has also become a focus of attention for quantum memory applications using the Zeeman levels of the $^4I_{15/2}$ ground state to build a three-level Λ system.[11–13] Using a Λ system, quantum information can be exchanged in a controlled fashion between the light fields and the material systems by optically coupling two $^4I_{15/2}$

ground-state Zeeman levels via a common single level of the $^4I_{13/2}$ excited-state multiplet. For $Er^{3+}:Y_2SiO_5$, a special direction of the magnetic field is required for both optical transitions in the two legs of the Λ system to have similar transition probabilities.[17] Long decoherence times of the transitions are also of great importance since decoherence of the optical and spin transitions limit how many single qubit operations can be performed and how long the quantum state can be stored. While choosing a magnetic field orientation where the Zeeman levels have small g factors can result in more favorable transition-probability ratios for the Λ system, we demonstrate that this is generally an uninviting scenario for achieving long decoherence times due to spectral diffusion from magnetic dipole-dipole (MDD) interactions.[15] Therefore, a compromise solution must be found.

In this paper, we extend previous material work on $Er^{3+}:Y_2SiO_5$ by directly studying how the choice of magnetic field orientation affects the decoherence properties of the Er^{3+} paramagnetic impurity ions. Two-pulse photon echo decays were measured for site 1 as a function of magnetic field orientation in the $\mathbf{D}_1$-$\mathbf{D}_2$ and $\mathbf{D}_2$-$\mathbf{b}$ optical extinction planes of the crystal. Furthermore, the evolution of decoherence was measured as a function of magnetic field orientation for site 2 in the $\mathbf{D}_1$-$\mathbf{D}_2$ plane by using stimulated-photon echo spectroscopy. We find that the decoherence times are strongly correlated with the corresponding ground- and excited-state g factor variations[16] for both Er^{3+} sites in these planes, with the observed decoherence times arising from the combined effects of the MDD coupling strength and the ground- and excited-state spin-flip rates along with the natural lifetime of the upper level. For some orientations, we expect the mutual spin flip-flops between Er ions could also contribute to the observed decoherence.

The low site symmetry of each Er^{3+} site, which leads to different g tensors for all the levels involved,[16] combined with the lack of knowledge of the angle dependence for a number of material properties, such as the anisotropic phonon coupling strength, make quantitative modeling of the observed behavior in $Er^{3+}:Y_2SiO_5$ challenging. As a result, the experimental findings are of particular interest in the context of developing a suitable optical Λ system in $Er^{3+}:Y_2SiO_5$ and for applications where extremely long decoherence times or correspondingly extremely narrow homogeneous linewidths are required. As we show in this paper, we were able to identify a preferred magnetic field orientation in the $\mathbf{D}_1$-$\mathbf{D}_2$ plane that allowed the measurement of a decoherence time of 4.38 ms, an exceptionally long value for a solid and corresponding to a homogeneous optical linewidth of 73 Hz. For perspective, the lifetime limit for this homogeneous linewidth is 14 Hz.

II. MATERIAL

Two $Er^{3+}:Y_2SiO_5$ crystals grown by the Czochralski method doped with 0.0015 at. % erbium concentration (growth number 1–544) and 0.005 at. % erbium concentration (growth number 7–167) were provided by Scientific Materials, Inc. (Bozeman, Montana). The structure of the host crystal Y_2SiO_5 is described by the space group C_{2h}^6 ($C2/c$, number 15) with 8 formula units per monoclinic cell. There are three mutually perpendicular optical extinction axes in Y_2SiO_5; the $\mathbf{b}$ axis is parallel to the $\langle 010\rangle$ direction and the $\mathbf{D}_1$ and $\mathbf{D}_2$ axes correspond to the optical extinction directions when the crystal is viewed along $\langle 010\rangle$ between crossed polarizers.[18] The crystals were oriented using x-ray diffraction, cut perpendicular to the three optical extinction axes, and polished to optical quality. The Y_2SiO_5 material is a well-known host for achieving ultraslow optical decoherence for several other rare-earth ions including Eu^{3+} (Ref. 19) and Pr^{3+} at low temperatures because the constituent elements in Y_2SiO_5 have small magnetic moments ($-0.137\mu_N$ for ^{89}Y) or small natural abundance of magnetic isotopes (4.7% with $-0.554\mu_N$ for ^{29}Si, 0.04% with $-1.89\mu_N$ for ^{17}O),[20] drastically reducing decoherence due to coupling of nuclear-spin fluctuations to the electronic levels.

The Y^{3+} ions occupy two crystallographically inequivalent sites of C_1 symmetry, and the Er^{3+} ions substitute for Y^{3+} host ions at both crystallographic sites without any need for charge compensation.[21] For each crystallographic site, four subclasses of sites with different orientations, related by the C_2 rotation and by inversion can be observed.[16] Subclasses related by inversion interact identically when a magnetic field is applied in an arbitrary direction making them magnetically equivalent, whereas those related by a C_2 rotation interact differently with the magnetic field and are thus magnetically inequivalent. In general, there are two magnetically inequivalent subclasses of sites for each crystallographic site; however, for the special cases of a magnetic field along the $\mathbf{b}$ axis or in the $\mathbf{D}_1$-$\mathbf{D}_2$ plane, all of the subclasses of a given site become magnetically equivalent. Magnetic equivalency of sites is desired for applications as it minimizes the overall doping concentration required for optical absorption, enhancing the interaction with the resonant optical field and increasing the overall Er^{3+}-Er^{3+} inter-ion distance, thereby reducing interactions that lead to spectral diffusion. Our present experiments focus on the case where the magnetic field was oriented in the $\mathbf{D}_1$-$\mathbf{D}_2$ plane where the two magnetically inequivalent sites become equivalent and large g factors for the ground and excited state were measured.[14,16] These experiments were contrasted with the case where the magnetic field was oriented in the $\mathbf{D}_2$-$\mathbf{b}$ plane where two magnetic inequivalent subclasses exist for each crystallographic site.

III. EXPERIMENT

The $Er^{3+}:Y_2SiO_5$ crystals were mounted on a rotating sample holder that allowed turning the sample in an Oxford Instruments SpectroMag cryostat in a constant horizontal magnetic field perpendicular to the laser beam as described in Ref. 16. The optical decoherence was characterized by measuring two-pulse and stimulated-photon echo decays as a function of magnetic field orientation in the $\mathbf{D}_1$-$\mathbf{D}_2$ plane for site 1 and site 2 at several magnetic fields at a temperature of $T=1.6$ K. For the ultraslow decoherence experiments, a magnetic field of $B=7$ T was oriented in the $\mathbf{D}_1$-$\mathbf{D}_2$ plane at an angle of 140° with respect to the $\mathbf{D}_1$ axis at a temperature of 1.5 K. We also measured two-pulse echo decays with the

magnetic field oriented in the $\mathbf{D}_2$-$\mathbf{b}$ plane for site 1 for a fixed magnetic field strength of $B=3$ T.

During sample mounting, a He-Ne laser beam was reflected off the crystal. Observation of any motion of the back-reflected light while the crystal was rotated was used to make small adjustments to the crystals' mounting until incident and reflected beams coincided during rotation. The optical extinction directions $\mathbf{D}_1$ and $\mathbf{D}_2$ were determined by viewing the crystal in the cryostat between crossed polarizers. For the case where the magnetic field is in the $\mathbf{D}_1$-$\mathbf{D}_2$ plane, all of the subclasses of a given crystallographic site become magnetically equivalent, and this information was used to fine tune the crystal alignment with respect to the magnetic field direction in the cryostat. For instance, if eight transitions were observed, the crystal holder alignment was corrected so that the eight transitions collapsed into four. Moreover, the $\mathbf{D}_1$ and $\mathbf{D}_2$ axes can be easily identified by rotating the crystal in the $\mathbf{D}_1$-$\mathbf{D}_2$ plane and observing the crossings of the lines for site 2 which locate the special $\Delta g=0$ directions for site 2 occurring for angles of 53° and 80°, respectively, with respect to the crystal $\mathbf{D}_1$ axis.[16]

With the magnetic field in the $\mathbf{D}_1$-$\mathbf{D}_2$ plane, clockwise and counterclockwise rotations of the field about the $\mathbf{b}$ axis are not equivalent. We adopted the sense of rotation defined in Ref. 16, where the angle between the magnetic field and the crystal axis is defined with respect to $\mathbf{D}_1$ in a counterclockwise sense. Similarly with the magnetic field in the $\mathbf{D}_2$-$\mathbf{b}$ plane, the magnetic field rotation is in a counterclockwise sense referenced with respect to the crystal $\mathbf{b}$ axis.

The relevant site 1 (site 2) $^4I_{15/2} \leftrightarrow {}^4I_{13/2}$ transition occurs at 1536.4776 ± 0.0004 nm (1538.9034 ± 0.0004 nm) in vacuum at zero magnetic field.[14] Application of a magnetic field lifts the Kramers degeneracy by splitting each doubly-degenerate crystal-field level. Experiments with the magnetic field in the $\mathbf{D}_1$-$\mathbf{D}_2$ plane and the laser beam propagating along $\mathbf{b}$ were carried out on the b line of site 1 and site 2 respectively; these correspond to the lowest to lowest transition between the Zeeman-split ground- and excited-state doublets.[14] For experiments with the magnetic field in the $\mathbf{D}_2$-$\mathbf{b}$ plane and the laser beam along $\mathbf{D}_1$, experiments were performed on the b line of magnetic subclass II of site 1, as defined in Ref. 16.

The laser source was a homemade external cavity diode laser in the Littman-Metcalf configuration with ~1.8 mW output power that seeded an erbium doped fiber amplifier providing ~15 mW of optical power at the sample. The absolute frequency of the diode laser was monitored with a wavemeter. For most experiments, the laser beam was focused inside the crystal to a waist of radius ~25 μm. An acousto-optic modulator gated the amplified continuous-wave laser beam to generate the optical pulses for the photon echo excitation pulse sequence, and the overall excitation sequence was repeated at a 10 Hz repetition rate to ensure complete relaxation of the excited states between measurements. Choosing typical pulse widths of ~500 ns length led to a ~2 MHz spectral width that prepared a relatively broad packet in the inhomogeneous line and relaxed the frequency stability requirements on the laser linewidth. Two-pulse photon echo decays were recorded as a function of pulse separation t_{12}, the delay between the first and second pulse in the two-pulse excitation sequence. Stimulated echo decays were recorded as a function of t_{12} for several fixed waiting times T_W, the time between the second and the third pulse, in order to probe the evolution of spectral diffusion. The observed photon echo signals were directly detected with a fast photodiode and displayed on a digital oscilloscope that was interfaced with a data-acquisition computer. All photon echo experiments were fully computer controlled.[22]

IV. RESULTS AND DISCUSSION

For two-pulse echoes, the observed decay shape is a function of the homogeneous linewidth as well as the magnitude, rate, and statistical nature of the spectral diffusion process. Because these different contributions cannot be separately extracted from the two-pulse echo decays, the simplest approach for analyzing the decay curves is to use the empirical Mims decay shape to determine the associated decoherence decay time T_M first proposed by Mims,[23] which is given by

$$I(t_{12}) = I_0 \cdot \exp\left\{2\left(\frac{2t_{12}}{T_M}\right)^x\right\}, \tag{1}$$

where I_0 is the initial echo intensity, t_{12} is the separation between pulses 1 and 2, the exponent x determines the shape of the decay curve, and the effective decoherence time T_M is the time over which the material coherence decays to $1/e$ of its initial electric field amplitude, or $1/e^2$ of its initial intensity.

To describe the behavior of the empirical parameter T_M in the presence of spectral diffusion, we must examine how T_M is influenced by the different material parameters. The relations may be derived from the physical model for the echo decay,[15] giving

$$T_M = \frac{2\Gamma_0}{\Gamma_{SD}R}\left(-1 + \sqrt{1 + \frac{\Gamma_{SD}R}{\pi\Gamma_0^2}}\right), \tag{2}$$

where Γ_0 is the linewidth in the absence of spectral diffusion, including effects such as the single-ion homogeneous linewidth and instantaneous spectral diffusion, Γ_{SD} is the full width at half maximum of the dynamic distribution of transition frequencies due to dipole-dipole interactions, and R is the rate of the spectral diffusion process given by the sum of upward and downward spin-flip transition rates of the perturbing spins.

Note that in the past $1/(\pi T_M)$ has often been plotted as an empirical linewidth; however, this "empirical" linewidth does not have a clear meaning in the presence of spectral diffusion. Only in the limit of $R \ll T_M$ and $\Gamma_0 \ll \Gamma_{SD}$ can we equate $1/(\pi T_M)$ as a true linewidth or for $\Gamma_{SD} \ll \Gamma_0$ when we have $T_M = T_2$. The choice between analyzing T_M or $1/(\pi T_M)$ is important since the two approaches are not equivalent: each method will accentuate and suppress different features and each data point will be effectively weighted differently in any fitting process. In particular, plotting $1/(\pi T_M)$ would tend to accentuate data points where the decays are very fast and the data are less reliable. We have chosen to analyze the T_M values directly in this work.

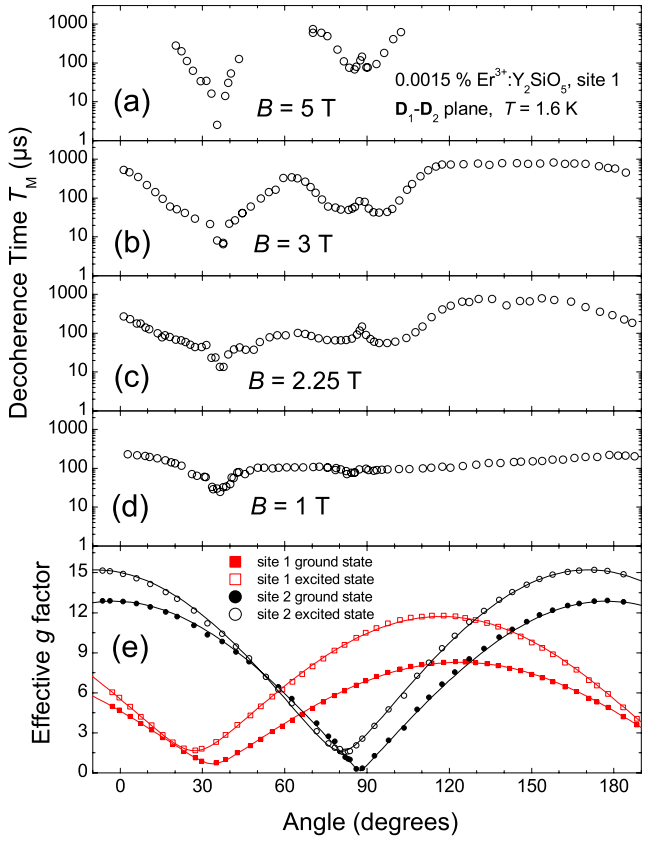

FIG. 1. (Color online) Two-pulse photon echo decoherence time T_M as a function of magnetic field orientation in the $\mathbf{D}_1$-$\mathbf{D}_2$ plane with the laser beam propagating along b for (a) $B=5$, (b) $B=3$, (c) $B=2.25$, and (d) $B=1$ T; the magnetic field angle was measured with respect to $\mathbf{D}_1$ in a counterclockwise sense, and the experiment was performed on the b line of the transition as defined in Ref. 14. (e) Corresponding effective g factor variations for site 1 (squares) and site 2 (circles) for the lowest-energy $^4I_{15/2}$ and $^4I_{13/2}$ states of $Er^{3+}:Y_2SiO_5$; ground-state solid symbols, excited-state open symbols. Solid lines are least-squares fits to the data showing excellent agreement.

A. Two-pulse echoes on site 1 with magnetic field orientation in $\mathbf{D}_1$-$\mathbf{D}_2$ plane

Figures 1(a)–1(d) show the $\mathbf{D}_1$-$\mathbf{D}_2$ plane results for crystallographic site 1 of the orientational dependent two-pulse photon echo measurements for magnetic fields $B=1$, 2.25, 3, and 5 T at $T=1.6$ K in 0.0015% $Er^{3+}:Y_2SiO_5$. In the figure, we plotted the decoherence time T_M of the b line[14] as a function of the angle the magnetic field makes with the $\mathbf{D}_1$ axis when the field is rotated with respect to $\mathbf{D}_1$ in a counterclockwise sense. Note that we only measured a few representative data points for $B=5$ T. For comparison, Fig. 1(e) shows the corresponding effective g factor variations for site 1 (squares) and site 2 (circles) for the lowest-energy $^4I_{15/2}$ and $^4I_{13/2}$ states of $Er^{3+}:Y_2SiO_5$ from Ref. 16. We have chosen solid symbols for the ground state and open symbols for the excited state. Solid lines in Fig. 1(e) are least-squares fits to the data described in Ref. 16, showing excellent agreement.

The variation in the decoherence time T_M with the orientation of the magnetic field arises from the combined effects of the transition's homogeneous linewidth, the MDD coupling strength, and the ground- and excited-state spin-flip rates. Ideally we would quantitatively model the observed angle dependence of the decoherence time T_M in Fig. 1 using Eq. (2), with known expressions for Γ_0, Γ_{SD}, and R from Ref. 15 and the functional form of the angular dependence of the g factors in that particular optical extinction plane shown in Fig. 1(e) from Ref. 16. However, in $Er^{3+}:Y_2SiO_5$, the interactions contributing to T_M are complicated by the presence of the two inequivalent sites with different magnetic properties and by the fact that the orientations of the principle axes of the g tensors are different for all of the levels involved in these processes.[16] In addition, because the two-pulse echo decay depends on the rate of spectral diffusion, we must have an accurate model for the anisotropy of the spin-flip rate in order to describe the angle dependence of the decoherence. We do not have any information about the spin-lattice relaxation mechanisms and rates for Er^{3+} ions residing at site 2, which is an important contribution to the angle dependence. We also do not know the strength of the site 1-site 1 Er^{3+}-Er^{3+} flip-flop rates, which undoubtedly play an important role in the decoherence for some field strengths and orientations. Furthermore, we expect the MDD tensor coupling and the phonon coupling coefficients to be anisotropic, requiring a full tensor treatment for the low-symmetry sites in Y_2SiO_5, but we only have measurements for the single orientation of $\mathbf{B}\|\mathbf{D}_1$ from Ref. 15. A simple scalar equation such as Eq. (2) cannot account for the full tensor nature of this interaction. In addition, at low-field magnitudes, high temperatures, or high concentrations, we may observe motional narrowing effects in the echo decays that correspond to Mims decay curves that have an exponent of less than one ($x<1$), requiring a different model to describe the echo decays. Thus, a detailed understanding of the precise structure and behavior of the orientation dependence of the decoherence will require further comprehensive measurements of material properties. Nevertheless, several important general conclusions can be drawn from the observed behavior based on the fundamental mechanisms responsible for the decoherence process in this material.

As shown in Figs. 1(a)–1(e) we observe a strong variation in the site 1 decoherence time T_M with the orientation of the magnetic field. As can be inspected from Eq. (2), the behavior of the decoherence time T_M is determined by the product of the magnitude of the spectral diffusion Γ_{SD} and the rate of the spectral diffusion R, which describes how fast the Er^{3+} spin population returns to thermal equilibrium. The functional form for Γ_{SD} is given by

$$\Gamma_{SD}(B,T) = \Gamma_{max}\,\mathrm{sech}^2\left(\frac{g_{env}\mu_B B}{2kT}\right), \tag{3}$$

where Γ_{max} is the full width at half maximum frequency broadening due to magnetic dipole-dipole interactions, g_{env} is the g factor of the perturbing magnetic moments, μ_B is the Bohr magneton, B is the magnetic field strength, k is the Boltzmann constant, and T is the temperature.[15] From Eq. (3), the magnitude of the spectral diffusion Γ_{SD} is entirely determined by the g factor of the perturbing spins if the temperature is held fixed. Ideally, to minimize decoherence,

the ground state should have the same g factor as the excited state for the optically active ion and the two magnetic-dipole moments should be parallel to make the optical transition insensitive to perturbations induced by electronic or nuclear-spin flips. For site 1, such special direction does not cross the $\mathbf{D}_1$-$\mathbf{D}_2$ plane.[16] Moreover, the environmental Er^{3+} ions in the lattice surrounding the optically active ions should have large ground-state g factors to freeze out the spin population in the upper Zeeman level and hence reduce the spin-flips causing spectral diffusion and decoherence. Indeed, as one can expect from Fig. 1, the longest decoherence times occurred in the region of $120°-150°$ where the g factors are maximized for both sites.

Even though these echo measurements were performed on site 1, the overall angle dependence requires taking into account all ions, including those residing at site 2. From Fig. 1, it can be seen that the decoherence time T_M exhibits two minima, one at $\sim 30°$ due to the g factors of site 1 undergoing a minimum, but also another at $\sim 90°$ where the g factors of site 2 are minimized. This behavior becomes more pronounced with increasing magnetic field strength.

We also need to consider the spectral diffusion rate R, which factors into the behavior of T_M as described by Eq. (2) as well as affecting the homogeneous linewidth due to variations in the spin-state lifetime.[15] There are several processes contributing to the spectral diffusion rate, the one-phonon direct process for spin-lattice relaxation involving absorption or emission of a single phonon resonant with the perturbing moment's spin-flip transition, the two-phonon Raman process in which the inelastic scattering of a high-energy phonon induces a transition between the spin states, the two phonon resonant Orbach process where the perturbing spin's state is changed through excitation to a low-lying crystal-field level by phonon absorption and relaxation to a different spin state through phonon emission, and mutual Er^{3+}-Er^{3+} spin flip-flops, where resonant pairs of antiparallel spins flip simultaneously.

For a single sample at a fixed temperature for the measured magnetic fields, we expect the overall spectral diffusion rate to be described by

$$R(B,T) = \alpha_D g_{\mathrm{env}}^3 B^5 \coth\left(\frac{g_{\mathrm{env}}\mu_B B}{2kT}\right) + \alpha_{\mathrm{ff}} g_{\mathrm{env}}^4 \operatorname{sech}^2\left(\frac{g_{\mathrm{env}}\mu_B B}{2kT}\right) + R_0, \quad (4)$$

where the Raman and Orbach contributions have been lumped into R_0 as they have no explicit dependence on the magnetic field strength (although they can generally depend on magnetic field orientation). The first term describes the direct one-phonon spin-flip process that often dominates the behavior at low temperatures and high magnetic fields, where α_D is a generally anisotropic constant characterizing the strength of the phonon coupling. The second term represents the average flip-flop rate for spins, where α_{ff} is a constant that depends on the details of the crystal structure and resonance line shape. Since the Er^{3+} ions are randomly distributed throughout the lattice, there will not be a single rate, but a distribution of flip-flop rates determined by the distribution of ion environments. The flip-flop rate also depends strongly on magnetic field orientation due to anisotropy of the g factors. In addition, for orientations and field strengths that result in energy-level splittings smaller than the magnetic inhomogeneity or available thermal energy, it is very important to consider additional contributions to the rate due to flip-flops between Er^{3+} ions and nonresonant nuclear and electronic spins in the lattice.

As can be seen from Eq. (4), the direct-phonon process causes the rate of the spectral diffusion R to rapidly increase with magnetic field strength due to an increase in the accessible density of phonon states degenerate with the splitting of the Zeeman levels, whereas the flip-flop processes decrease rapidly with increasing field due to the reduced number of antiparallel spin pairs available. As mentioned before, we expect the individual rates to be very anisotropic through α_D, α_{ff}, and g_{env}, and additional material information is required to model the angular behavior in detail.

In general, it is the interplay between the magnitude of the spectral diffusion Γ_{SD} and the rate of the spectral diffusion R that predominantly determines the overall observed behavior for the decoherence time T_M. As our results show, the g factor variations serve as a reliable guide to determine special directions for applying an external magnetic field in this plane. Specifically, large g factors for both sites in the region between $120°$ and $150°$ lead to freezing out electron-spin fluctuations and reduced magnetic ion-ion interactions and consequently long decoherence times.

B. Two-pulse echoes on site 1 with magnetic field orientation in $\mathbf{D}_2$-b plane

Figure 2(a) shows the two-pulse echo decoherence time T_M for site 1 as a function of the angle that the magnetic field makes with the **b** axis when the field is rotated with respect to **b** in a counterclockwise sense in the $\mathbf{D}_2$-**b** plane; the laser beam was propagating along $\mathbf{D}_1$. Measurements were performed for a fixed magnetic field of $B=3$ T at a temperature of $T=1.6$ K in 0.005% $Er^{3+}:Y_2SiO_5$. The situation in the $\mathbf{D}_2$-**b** optical extinction plane is more complicated because magnetic subclasses are not degenerate as in the $\mathbf{D}_1$-$\mathbf{D}_2$ plane investigated before; we performed the echo measurements on the b line[14] of the magnetic subclass II of site 1 following the labeling scheme of Ref. 16. Figures 2(b) and 2(c) show the corresponding effective g-factor variations for the lowest-energy $^4I_{15/2}$ and $^4I_{13/2}$ states of $Er^{3+}:Y_2SiO_5$ in the $\mathbf{D}_2$-**b** plane for site 1 in (b) and for site 2 in (c). As in Fig. 1 we have chosen solid symbols for the ground state and open symbols for the excited state. Solid lines in Figs. 2(b) and 2(c) are least-squares fits to the data described in Ref. 16 showing excellent agreement.

As evident from Figs. 2(b) and 2(c), there is no magnetic field direction in this optical extinction plane that simultaneously maximizes the g factors for all site orientations and consequently optimizes the decoherence properties. The observed echo strengths for the field in this plane were considerably weaker and the decoherence times shorter due to the higher 0.005 at. % Er^{3+} concentration as well as the magnetic inequivalency of the Er^{3+} ions. As can be seen from

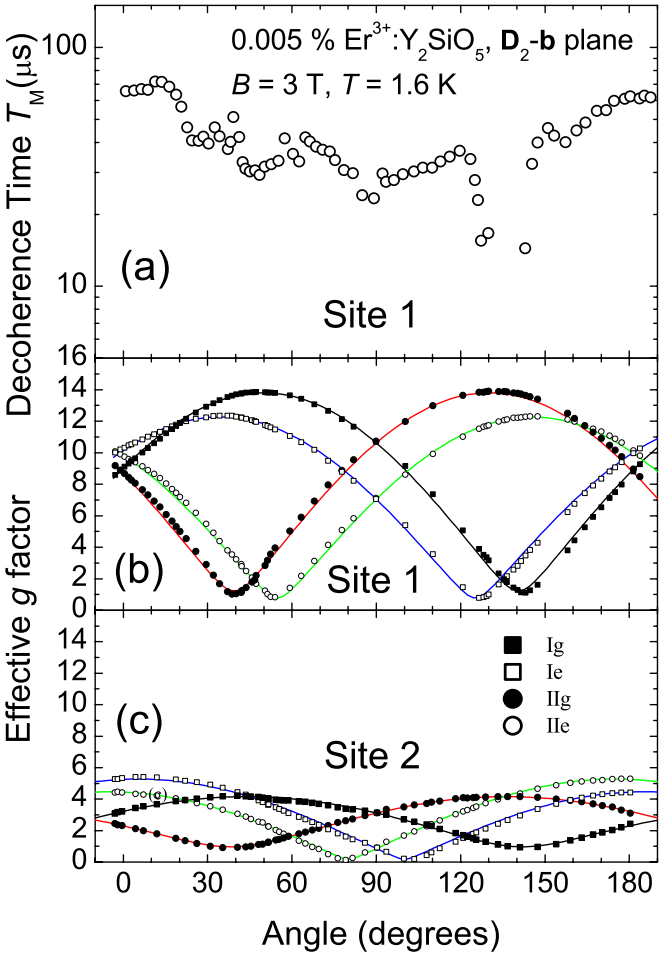

FIG. 2. (Color online) (a) Two-pulse photon echo decoherence time T_M for site 1 as a function of magnetic field orientation in the **b**-$\mathbf{D}_2$ plane with the laser beam propagating along $\mathbf{D}_1$ for $B=3$ T at $T=1.6$ K, experiments were performed on the magnetic subclass II of site 1 as defined in Ref. 16. Corresponding effective g factor variations for the lowest-energy $^4I_{15/2}$ and $^4I_{13/2}$ states of $Er^{3+}:Y_2SiO_5$ in the **b**-$\mathbf{D}_2$ plane are shown for site 1 in (b) and for site 2 in (c); ground-state solid symbols, excited-state open symbols. Solid lines are least-squares fits to the data showing excellent agreement.

Fig. 2(a) the longest decoherence times were measured near 0° and 180° where the magnetic field was oriented along **b** and the g factors of all orientations were relatively large. In contrast, no echo signal was detectable between 130° and 140° when the ground- and excited-state g factors for subclass II of site 1 were at their minima and the corresponding site 2 g factors were also small. Site 2 ions also contributed to the observed decoherence time as the local minimum near ~85° suggests.

C. Stimulated echoes on site 2 with magnetic field orientation in $\mathbf{D}_1$-$\mathbf{D}_2$ plane

To determine the effect of orientation on the spectral diffusion rate, stimulated photon echo decays were studied for site 2 on the b line in a 0.005% $Er^{3+}:Y_2SiO_5$ crystal as a function of magnetic field orientation in the $\mathbf{D}_1$-$\mathbf{D}_2$ plane

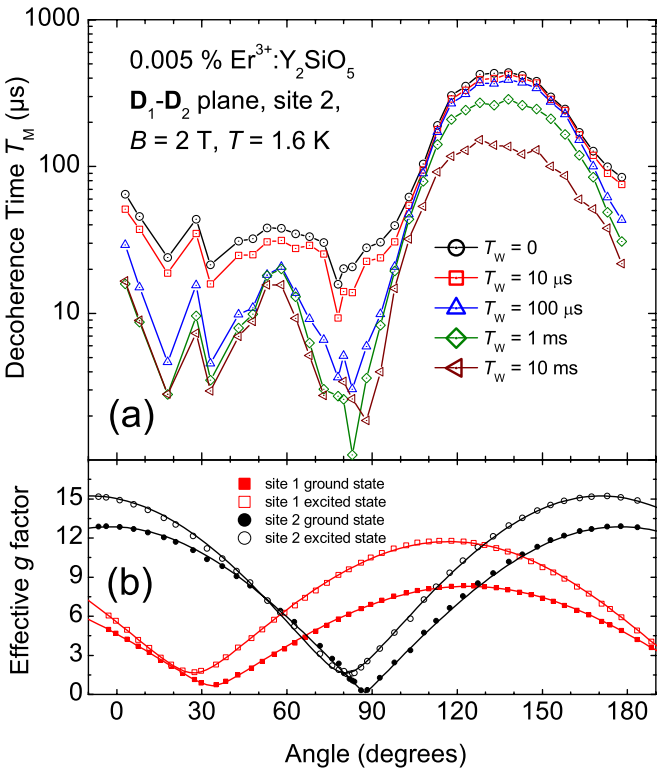

FIG. 3. (Color online) (a) Time evolution of the stimulated-photon echo decoherence time T_M for site 2 as a function of magnetic field orientation in the $\mathbf{D}_1$-$\mathbf{D}_2$ plane with the laser beam propagating along b for $B=2$ T and $T=1.6$ K for waiting times of $T_W=0$ (two-pulse echo), 10 μs, 100 μs, 1 ms, and 10 ms; the magnetic field angle was measured with respect to $\mathbf{D}_1$ in a counterclockwise sense and the experiment was performed on the b line of the transition. (b) Corresponding effective g factor variations for site 1 (squares) and site 2 (circles) for the lowest-energy $^4I_{15/2}$ and $^4I_{13/2}$ states of $Er^{3+}:Y_2SiO_5$; ground-state solid symbols, excited-state open symbols. Solid lines are least-squares fits to the data showing excellent agreement.

using a range of waiting times T_W. Figure 3 shows the time evolution of the stimulated photon echo decoherence time T_M as a function of magnetic field orientation for a fixed magnetic field of $B=2$ T, temperature of $T=1.6$ K, and waiting times of $T_W=0$ (two-pulse echo), 10 μs, 100 μs, 1 ms, and 10 ms. Figure 3(b) is identical to Fig. 1(e) and shows the corresponding effective g factor variations for site 1 (squares) and site 2 (circles) for comparison with the plots of Fig. 3(a). We observe a pronounced correlation between the g factor variation in the $\mathbf{D}_1$-$\mathbf{D}_2$ plane and the observed decoherence time. As expected, the longest decoherence times were measured where the g factors for both sites are large, which occurs for angles between 120° and 150°. For site 2 there are also two special directions in the $\mathbf{D}_1$-$\mathbf{D}_2$ plane for which the ground and excited g factors are exactly the same. These directions occur for angles of 53° and 80°, respectively.[16] In contrast to the predictions of simple magnetically isotropic models that would predict strong suppression of spectral diffusion, we only observe slightly longer decoherence times near 53°, but not near 80°. This result highlights the complexity of the MDD interaction in the low-

symmetry Y_2SiO_5 host, where the ground-state and excited-state magnetic moments are not parallel to each other and, even though the external field projections are the same, the moments interact differently with the environmental field fluctuations.

The influence of the optically active site 2 ions can be seen at the local minimum of T_M near 90°, where the site 2 g factors also go through a minimum. The presence of spectral diffusion is evident from the increase in decoherence, which is especially evident in the region between 120° and 150° where the decoherence time decreases from ~430 to 150 μs over a period of 10 ms that is near the excited-state lifetime of 9.2 ms.[14] From the data, it is also evident that the rate of spectral diffusion is highly anisotropic as a function of magnetic field orientation due to the anisotropies in the spin-flip mechanisms.

V. ULTRASLOW DECOHERENCE

Guided by the results of our two-pulse photon echo study as a function of magnetic field orientation in the $\mathbf{D}_1$-$\mathbf{D}_2$ plane, we investigated the material decoherence time under optimum experimental operating conditions for suppression of optical decoherence. Decoherence for site 1 was investigated using two-pulse photon echo measurements at a magnetic field of 7 T applied in the $\mathbf{D}_1$-$\mathbf{D}_2$ plane and with the laser propagation direction along **b**. According to Fig. 1(b) for $B=3$ T, consistently long T_M values were measured when the magnetic field was oriented in the $\mathbf{D}_1$-$\mathbf{D}_2$ plane at angles between 120° and 150°. Hence, we chose an angle of 140° for the magnetic field with respect to the $\mathbf{D}_1$ crystal axis. To "freeze out" thermal populations in the upper Zeeman level of the ground state, the sample was immersed in a liquid-helium bath pumped to 1.5 K. At the high magnetic field strength of 7 T and temperature of 1.5 K, spectral diffusion due to the electron-spin contribution was quenched.[15] Figure 4 shows the measured two-pulse echo decay under these conditions plotted on a semilogarithmic scale. The absence of spectral diffusion is evident in the single exponential behavior of the echo decay; scatter in the data after a time delay between the exciting pulses of $t_{12}\sim 1$ ms can be attributed to laser frequency instability. When laser frequency jitter exceeds the Fourier width of the exciting pulses, the second pulse fails to overlap spectrally with the first pulse resulting in a reduced echo signal; photon echo signal fidelity can be improved using a laser frequency-stabilized to a spectral hole.[1–4] With the absence of spectral diffusion, i.e. $R \ll T_M$ and $\Gamma_0 \ll \Gamma_{SD}$, the echo decay was described by a single exponential, so the Mims exponent x in Eq. (1) is equal to 1 and the empirical decoherence time T_M directly corresponds to the traditional optical T_2. For this special case, we can equate $1/(\pi T_M)$ to the true homogeneous linewidth.

The solid line in Fig. 4 shows a single exponential least-squares fit to the two-pulse photon echo decay curve giving an optical T_2 of 4.38 ms, which corresponds to an optical homogeneous linewidth of 73 Hz. This T_2 is an extraordinarily long optical decoherence time for a solid-state material, with the corresponding linewidth being an exceptionally narrow optical resonance. Residual contributions to this narrow linewidth are due to population decay, excitation induced decoherence (instantaneous spectral diffusion),[24] and contributions from the ^{89}Y nuclear-spin fluctuations.[15] The excited-state lifetime of $T_1=11.4$ ms establishes the ultimate limit of 14 Hz for the homogeneous linewidth in $Er^{3+}:Y_2SiO_5$.[5,14] Further measurements are required to separate those individual contributions, which may also include fluctuations in laser frequency stability, fluctuations of background magnetic fields, and stray electromagnetic fields in the laboratory as suggested by the results of Equall *et al.*[19]

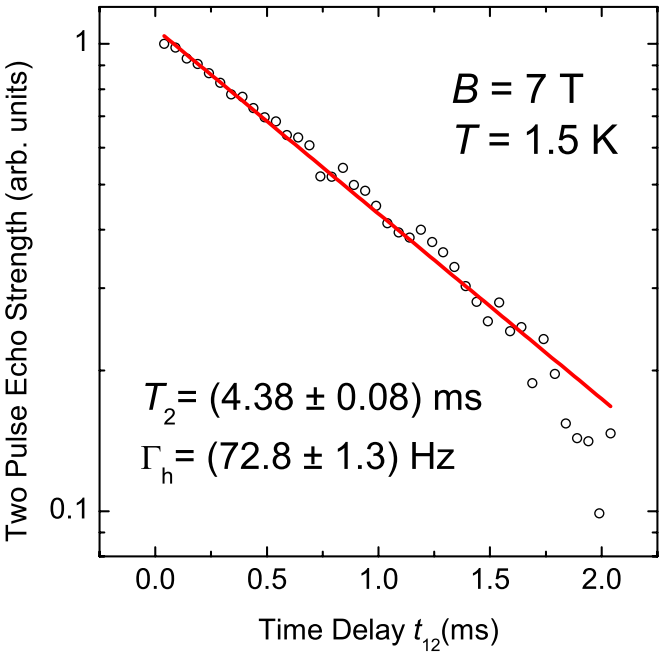

FIG. 4. (Color online) Two-pulse photon echo decay in 0.0015% $Er^{3+}:Y_2SiO_5$ at $B=7$ T and $T=1.5$ K. The lasers k vector is along **b** and **B** is oriented in the $\mathbf{D}_1$-$\mathbf{D}_2$ plane at an angle of 140° with respect to the $\mathbf{D}_1$ axis. The solid line represents an exponential least square fit to the data yielding a decoherence time of $T_2=4.38$ ms which corresponds to a homogeneous linewidth of 73 Hz.

VI. SUMMARY

In summary, we measured the magnetic field orientation dependence of the decoherence time for the $\mathbf{D}_1$-$\mathbf{D}_2$ and $\mathbf{D}_2$-**b** planes and compared the data to the corresponding g factor variations in these planes. The rotational g factor variation of both crystallographic sites provided a reliable guide for choosing the external magnetic field orientation in reducing optical decoherence. Optical decoherence can be efficiently suppressed by requiring large g factors. As the experimental results showed, environment ions residing in both crystallographic sites contributed to decoherence and all sites thus have to be considered in the selection of a preferred external magnetic field orientation. The longest decoherence times were measured in the optical $\mathbf{D}_1$-$\mathbf{D}_2$ crystal plane along a magnetic field direction offset from the $\mathbf{D}_1$ axis by an angle of $\sim 120° - 150°$ for site 1 as well as site 2. This direction gave overall maxima of g factors for both crystallographic

sites that, in addition, have the advantage of being magnetically equivalent. Orientational dependent two-pulse echo measurements in the $\mathbf{D}_2$-**b** plane strongly supported those results; there the multitude of magnetically inequivalent Er^{3+} ions hindered the ability to find simultaneous *g* factor maxima, and the observed echo strengths consequently were weaker and the decoherence times were significantly shorter.

At this time, additional work is required to complete the quantitative description of the experimental data because of the complexity associated with the low symmetry of the $Er^{3+}:Y_2SiO_5$ material system where information on anisotropic spin-lattice relaxation rates and anisotropic MDD coupling for both sites would be required. With those additional details of anisotropic relaxation rates and MDD interactions, we expect that the decoherence behavior as a function of direction and magnitude of the applied field could be described and predicted in detail.

The experimental measurements reported here are directly relevant to development of SSH materials and optical Λ systems for quantum memory. From our results, we find that decoherence is generally minimized by employing materials with weakly magnetic or nonmagnetic host constituents (such as Y_2SiO_5) and then choosing magnetic field orientations where both the excited and ground state *g* factors of the active ion and the *g* factors of any other perturbing environmental spins are all simultaneously maximized. In addition, to optimize the performance of Λ systems for quantum information applications, we would also seek to choose orientations where the ground- and excited-state magnetic moments are nearly orthogonal to each other to optimize the transition-probability ratio for the two legs of the Λ system. In contrast, for applications that employ a single transition, such as SSH, we would seek to choose orientations where the ground- and excited-state magnetic moments are parallel to each other to minimize sensitivity to environmental field fluctuations. By identifying optimal magnetic field orientations in $Er:Y_2SiO_5$, these studies also enabled the measurement of an extraordinarily narrow optical resonance in a solid with a homogeneous linewidth of 73 Hz.

ACKNOWLEDGMENTS

The authors are grateful to R. W. Equall and R. L. Hutcheson of Scientific Materials Corporation of Bozeman, Montana for providing the crystals. This research was supported by the Air Force Research Laboratory through AFOSR Grant No. F49620-00-1-0314 and by DARPA Grant No. MDA972-03-1-0002. T.B. wishes to acknowledge financial support from the University of San Francisco Faculty Development Fund.

*Permanent address: Department of Physics and Astronomy, University of San Francisco, 2130 Fulton Street, San Francisco, California 94117, USA; tbottger@usfca.edu

†thiel@physics.montana.edu

‡cone@montana.edu

§Permanent address: Department of Physics, University of South Dakota, Vermillion, South Dakota 57069, USA; ycsun@usd.edu

[1] P. B. Sellin, N. M. Strickland, T. Böttger, J. L. Carlsten, and R. L. Cone, Phys. Rev. B **63**, 155111 (2001).

[2] Thomas Böttger, Y. Sun, G. J. Pryde, G. Reinemer, and R. L. Cone, J. Lumin. **94-95**, 565 (2001).

[3] G. J. Pryde, T. Böttger, and R. L. Cone, J. Lumin. **98**, 309 (2002).

[4] Thomas Böttger, G. J. Pryde, and R. L. Cone, Opt. Lett. **28**, 200 (2003).

[5] Thomas Böttger, Y. Sun, C. W. Thiel, and R. L. Cone, Proc. SPIE **4988**, 51 (2003).

[6] Z. Cole, T. Böttger, R. Krishna Mohan, R. Reibel, W. R. Babbitt, R. L. Cone, and K. D. Merkel, Appl. Phys. Lett. **81**, 3525 (2002).

[7] T. L. Harris, Y. Sun, R. L. Cone, R. M. Macfarlane, and R. W. Equall, Opt. Lett. **23**, 636 (1998).

[8] T. L. Harris, Y. Sun, W. R. Babbitt, J. A. Ritcey, and R. W. Equall, Opt. Lett. **25**, 85 (2000).

[9] V. Crozatier, V. Lavielle, F. Bretenaker, J.-L. Le Gouët, and I. Lorgeré, IEEE J. Quantum Electron. **40**, 1450 (2004).

[10] Thomas Böttger, C. W. Thiel, R. L. Cone, and Y. Sun, Phys. Rev. B **77**, 155125 (2008).

[11] O. Guillot-Noël, Ph. Goldner, Y. Le Du, E. Baldit, P. Monnier, and K. Bencheikh, Phys. Rev. B **74**, 214409 (2006).

[12] S. R. Hastings-Simon, B. Lauritzen, M. U. Staudt, J. L. M. van Mechelen, C. Simon, H. de Riedmatten, M. Afzelius, and N. Gisin, Phys. Rev. B **78**, 085410 (2008).

[13] W. Tittel, M. Afzelius, R. L. Cone, T. Chanelière, S. Kröll, S. A. Moiseev, and M. Sellars, arXiv:0810.0172v1, Laser Photonics Rev. (to be published).

[14] Thomas Böttger, Y. Sun, C. W. Thiel, and R. L. Cone, Phys. Rev. B **74**, 075107 (2006).

[15] Thomas Böttger, C. W. Thiel, Y. Sun, and R. L. Cone, Phys. Rev. B **73**, 075101 (2006).

[16] Y. Sun, Thomas Böttger, C. W. Thiel, and R. L. Cone, Phys. Rev. B **77**, 085124 (2008).

[17] C. W. Thiel, M. Afzelius, and R. L. Cone (unpublished).

[18] C. Li, C. Wyon, and Richard Moncorge, IEEE J. Quantum Electron. **28**, 1209 (1992).

[19] R. W. Equall, Y. Sun, R. L. Cone, and R. M. Macfarlane, Phys. Rev. Lett. **72**, 2179 (1994).

[20] R. M. Macfarlane, T. L. Harris, Y. Sun, R. L. Cone, and R. W. Equall, Opt. Lett. **22**, 871 1997.

[21] B. A. Maksimov, Yu. A. Kharitonov, V. V. Ilyukhin, and N. B. Belov, Sov. Phys. Dokl. **13**, 1188 (1969).

[22] Data acquisition software by C. W. Thiel.

[23] W. B. Mims, Phys. Rev. **168**, 370 (1968).

[24] G. K. Liu and R. L. Cone, Phys. Rev. B **41**, 6193 (1990).